Development of all metal electrothermal actuator and its applications

JiKui (Jack) Luo
Johnny H. He
Andrew Flewitt
D. F. Moore
University of Cambridge
Department of Engineering
Cambridge, CB2 1PZ
United Kingdom

S. Mark Spearing
Massachusetts Institute of Technology
Department of Aeronautics & Astronautics
Cambridge, Massachusetts 02139

Norman A. Fleck
W. I. Milne
University of Cambridge
Department of Engineering
Cambridge, CB2 1PZ
United Kingdom

Abstract. The in-plane motion of microelectrothermal actuator ("heatuator") has been analyzed for Si-based and metallic devices. It was found that the lateral deflection of a heatuator made of a Ni metal is about ~60% larger than that of a Si-based actuator under the same power consumption. Metals are much better for thermal actuators as they provide a relatively large deflection and large force, for a low operating temperature and power consumption. Electroplated Ni films were used to fabricate heatuators. The electrical and mechanical properties of electroplated Ni thin films have been investigated as a function of temperature and plating current density, and the process conditions have been optimized to obtain stress-free films suitable for microelectromechanical systems applications. Lateral thermal actuators have been successfully fabricated, and electrically tested. Microswitches and microtweezers utilizing the heatuator have also been fabricated and tested.
© *2005 Society of Photo-Optical Instrumentation Engineers.* [DOI: 10.1117/1.1898243]

Subject terms: finite element analysis; metal thermal actuator; electroplating; Ni; heatuator; electrothermal actuator; microswitch; microtweezers.

Paper 04010 received Mar. 16, 2004; revised manuscript received Sep. 2, 2004; accepted for publication Sep. 3, 2004; published online May 17, 2005. This paper is a revision of a paper presented at the SPIE conference on MEMS/MOEMS Components and their Applications, Jan. 2004, San Jose, California. The paper presented there appears (unrefereed) in SPIE Proceedings Vol. 5344.

1 Introduction

In order to realize the integration of microelectromechanical systems (MEMS) with complementary metal oxide semiconductor (CMOS), small scale, low process temperature, low power consumption, low operating voltage, and temperature are essential for MEMS devices and microfabrication processes. Electrostatic MEMS actuators are small in size with limited displacements and forces, whereas thermal actuators can produce larger forces and displacements. Two types of thermal actuators are well studied; one is the out-of-plane motion, vertical thermal actuator based on the thermal expansion difference between two materials of a bilayer structure,[1] and the other is the in-plane motion, lateral thermal actuator based on the thermal expansion difference caused solely by temperature differences within a monolithic structure,[2–6] this latter type of device is sometimes called a "heatuator." Currently lateral thermal actuators are typically made from polysilicon films, which need a high operating temperature to produce sufficient force and displacement owing to the small thermal expansion coefficient of Si. Further, a long time, high temperature annealing step ($>1000\,°C$) is needed to minimize the residual stress in polysilicon films,[7] suitable for MEMS fabrication. These factors limit the possible polysilicon MEMS devices that can be integrated with CMOS, particularly on top of CMOS, as the high operating temperature heats the chips above the limitation of the Si substrate, and produces a large quantity of heat, further worsening the cooling problems for chips. High temperature annealing makes the full integration of MEMS on top of CMOS difficult, as it destroys the circuits beneath. On the other hand, metal can be deposited during the backend process without involving any high temperature process. Metal thermal actuators can be operated at much lower temperature owing to their much larger thermal expansion coefficients. Metal thermal actuators are expected to be one of the most important branches of the MEMS family of devices, particularly for those integrated with CMOS.

Electroplating provides a simple and low-cost technique to produce high quality metal films suitable for MEMS applications. This technique can now be easily integrated with CMOS technology. Sensors and actuators based on plated metals have been widely fabricated and studied such as a thermal actuator, microcoil, micromotor, and pneumatic actuator.[8–15] Ni and NiFe metals are most commonly used for MEMS devices.

In this paper, we will report analytical and finite element simulation results for electrothermal actuators, investigation of material properties of electroplated Ni films as a function of temperature and current density, and the development of metal electrothermal actuators.

2 Theoretical Analysis and Simulation

2.1 *Thermal Conduction Model and Material Selection*

For surface microtechnology or the integration of MEMS devices with CMOS, in-plane motion thermal actuators are preferred; here we consider the lateral thermal actuator as shown in Fig. 1(a). The heatuator consists of a thin hot arm, a wide cold arm, and a hinge. When a current is passed

1537-1646/2005/$22.00 © 2005 SPIE

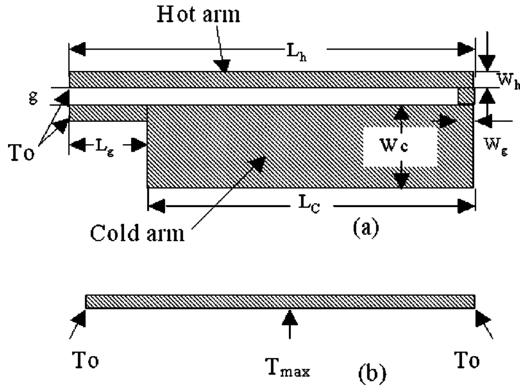

Fig. 1 (a) Schematic drawing of lateral motion electrothermal actuator and (b) a simplified 1-D model for thermal conduction analysis.

through from one terminal to another, the thin (high electrical resistance) hot arm is heated up more than the wide (low electrical resistance) cold arm, thus the hot arm expands more than the cold arm, generating a lateral deflection (or displacement). We will analyze how the material properties affect the thermal actuator performance, e.g., the deflection, as it is more important than the force for most applications under consideration.

For the temperature range $<700\,°C$ we are interested, it is reasonable to assume that convection and radiation make little contribution to thermal losses.[16] Under the one-dimensional assumption, the temperature of the heatuator at steady state is then governed by the basic heat transfer equation[5,6]:

$$k\frac{d^2T}{dx^2}+J^2\rho=0, \tag{1}$$

$$J=\frac{E_F}{\rho}, \tag{2}$$

where J is the current density, E_F the electrical field, $E_F=V/L$, V the applied voltage, L the length of the resistor, ρ the resistivity, and k the thermal conductivity.

In order to develop an analytical model, we further simplify the device structure. When the width of the cold arm is much wider than the hot arm, e.g., $W_c/W_h>20$, the temperature of the cold arm is close to the environment. Assuming the cold arm is infinitely wide, and then its temperature does not change with the applied voltage. Thus the problem is simplified to be a single hot beam with both ends as heat sinks at an ambient temperature T_0, as shown in Fig. 1(b).

Integrating Eq. (1), and applying boundary conditions $T=T_0$ at $X=0$ and $X=L$, we have the temperature distribution along the beam as

$$T(x)=\frac{\rho J^2}{2k}(Lx-x^2)+T_0. \tag{3}$$

The maximum temperature is in the middle of the beam, and the average temperature ΔT_{ave} of the beam is given by

$$\Delta T_{ave}=\int\frac{T(x)-To}{L}dx=\frac{1}{12}\frac{V^2}{k\rho}=\frac{PL}{12kA}, \tag{4}$$

where $P=IV$ the consumed power. Here $I=JA$ is the current and A is the cross section of the beam. Given that the deflection d of the beam is proportional to the temperature difference between the cold and the hot arms, and is inversely proportional to the flexural rigidity as follows[5,6]:

$$d\propto\frac{\alpha\Delta T_{ave}}{E}=\frac{\alpha V^2}{12k\rho E}=\frac{\alpha}{kE}\frac{PL}{12A}=\frac{QPL}{12A}, \tag{5}$$

where α is the thermal expansion coefficient and E is Young's modulus. Provided that all material properties are independent of temperature, and the power and the device dimensions are fixed, the deflection of a heatuator is therefore proportional to $Q=\alpha/kE$. Q is a figure of merit for material selection, solely depending on the material's properties. In reality the heatuator operates with a combined, axial-bending displacement of the hot arm, but the figure of merit is still valid, only the numerical coefficient changes. Table 1 summarizes the material properties and the figure of merit for poly-Si and several metals. For the same power, the Q of a Ni-thermal actuator is ~60% better than that of a Si-based thermal actuator. Alternatively, the Si-based actuator needs ~60% more power to deliver a similar amount of deflection.

It is interesting to compare different metals for use in heatuators. Tungsten has a very large Young's modulus, but Q is almost one order of magnitude smaller than for other materials. Copper has a higher thermal expansion coefficient, but because of the large thermal conductivity, it is worse for a heatuator. Aluminum is a good material for a heatuator, but its yield strength is too small and it deforms easily at high operating temperature. Among those metals

Table 1 Material properties and quality factor (Refs. 1–6 and 17–19).

Material	α (10^{-6}/°C)	ρ 10^{-8} (Ω m)	k (W/M °C)	E (GPa)	Q (10^{-19})	σ_y (MPa)
Ni	12.7	6.84	83	210	7.65	221–572
Poly-Si	2.6	~1000	34	160	4.75	···
W	4.4	5.9	140	360	0.873	4000
Al	23	3.3	155	69	8.33	170
Cu	17	1.7	400	110	3.86	100

Table 2 Material properties of Ni and poly-Si.

Material	α 10^{-6} (/°C)	ρ 10^{-8} (ΩM)	k (W/MC)	E (GPa)	ξ 10^{-3} (/°C)
Ni	12.7	20	83	210	3.0
Poly-Si	2.6	1000	34	160	−0.35

presently suitable for microsystems, Ni has superior properties for the purposes of heatuators, and is the material upon which the present work is focused. Also stress-free Ni thin films, suitable for MEMS applications can be easily obtained by electroplating, without needing a high temperature process.

Since the resistivity of the materials is temperature dependent, typically varying with T as $\rho=\rho_0[1+\xi(T-T_0)]$, we have to assess the effect of the temperature coefficient ξ, of resistivity on the performance of the thermal actuator. ξ of polysilicon is in the range from -1.2×10^{-3} to 1.2×10^{-3}/°C, and it decreases when the doping level is increased.[17] In general, ξ of poly-Si is negative for the doping levels and the temperatures of interest. On the other hand, ξ of metals is positive. Assuming that the power levels are the same for two identical heatuators made of poly-Si and Ni, under a bias the hot arm temperature of a metal heatuator is much higher than the cold arm, thus the resistance of the hot arm increases faster than that of the cold arm for metals, as a consequence, more power is consumed by the hot arm, and then a larger deflection is obtained. For poly-Si, as $\xi_{\rm poly}$ is typically negative, the resistance of its hot arm decreases under an applied voltage, leading to less power, thus less deflection. This implies that the Ni hot arm has the highest power consumption, whereas the Ni cold arm has the lowest power. Because of the higher power difference, the Ni actuator will deliver much more deflection than the poly-Si heatuator. The above-mentioned analysis indicates that metals are much better than silicon for thermal actuator applications.

2.2 *Finite Element Simulation*

In order to examine the quantitative difference between metal and poly-Si heatuators, finite element numerical simulation based on *FEMLAB* software (a commercially available plug-in software for MATLAB, The MathWork, Inc., 3 Apple Hill Drive, Natick, MA 01760-2090, USA) was used to model the device performance. Material properties and the heatuator dimensions are summarized in Tables 2 and 3. The values of the resistivity and its temperature coefficient for Ni were obtained experimentally as will be described later. Owing to the lack of measurement technique here, the thermal conductivity k was kept unchanged. The thermal conductivity k and resistivity are correlated through the Wiedemann–Franz law, and the thermal conductivity decreases as the resistivity increases.[20] However it is understood from the Q definition that Q increases when k becomes smaller; a better performance of the heatuator is expected if a lower thermal conductivity is used. Therefore the use of experimental resistivity for the simulation does not change the results qualitatively, but quantitatively, and will not change the conclusion of this research. Since we try to discuss material selection for heatuators, once again the heat loss through the convection and radiation are also ignored in the finite element simulation, as they have the same effect on the device structure made from different materials.

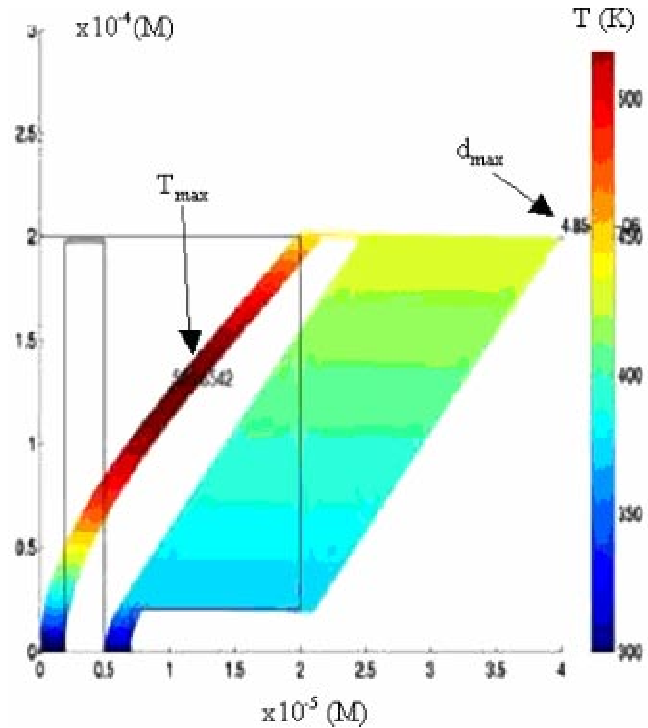

Fig. 2 The simulated displacement and temperature distribution for a Ni-heatuator at 0.2 V bias. $T_{\rm max}$ are ~250 °C (524 K) with a displacement of 4.9 μm. The displacement is not scaled.

Figure 2 shows the simulated displacement and temperature distribution of Ni-thermal actuator under 0.2 V applied voltage using *FEMLAB*. *FEMLAB* software has provided a tool to optimize the mesh density for an accurate simulation. Nevertheless we have also carefully checked the effect of the mesh density on the simulation results. For example, 1275 mesh elements have been used to simulate the device shown in Fig. 2; when the mesh elements increased to 5100, the difference was less than 0.1% for the maximum temperature and the displacement, sufficiently accurate for the modeling.

At a maximum temperature of ~250 °C, the device delivers a displacement of ~4.9 μm, for the same amount of

Table 3 Device parameters used for simulation.

L_h (μm)	L_c (μm)	L_g (μm)	W_h (μm)	W_c (μm)	W_g (μm)	g (μm)	t (μm)
200	180	20	2	15	3	2	2

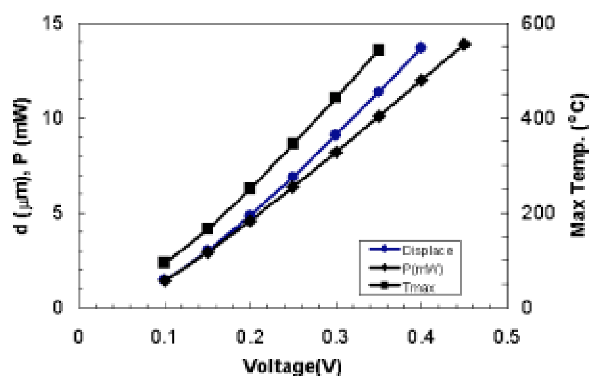

Fig. 3 Simulated displacement, power consumption and T_{max} for Ni actuator as a function of bias.

displacement, a maximum temperature of ~1100 °C is required for a poly-Si heatuator. This difference in displacement increases with increasing the operating temperature. Figures 3 and 4 are the simulated results of the deflections, the powers and the maximum temperatures for Ni and poly-Si thermal actuators with the same dimensions. The power was calculated based on the applied voltage and the resistance obtained using the resistivity at the average raised temperature ΔT_{ave}. For the polysilicon actuator, a temperature over 900 °C is needed to obtain a reasonable displacement (>5 μm) and force, whereas for a similar amount of displacement, Ni actuators need a much lower operating temperature, around 250 °C. Also it reveals that for the same amount of deflection, for instance 5 μm, the power consumed for the Si actuator is more than double that of the Ni actuator, though it strongly depends on the resistivity of the active materials. The simulation results demonstrate that the metal actuator has a much lower operating temperature and power consumption, for a given displacement than Si-based devices, which is consistent with the analytical results.

3 Fabrication and Measurements

Electroplated Ni thin films were used for the fabrication of electrothermal actuators. These were plated using a nickel sulfamate solution, containing 300 g/L nickel sulfamate, 10 g/L nickel chloride, and 40 g/L boric acid at a temperature between 20 and 80 °C. A magnetic pellet was used to stir the solution to maintain the uniformity of the concentration. The plating current density was varied in the range of 1–30 mA/cm^2 as part of a process optimization study. Before the fabrication of actuators, the materials properties were first investigated and then used in the simulations.

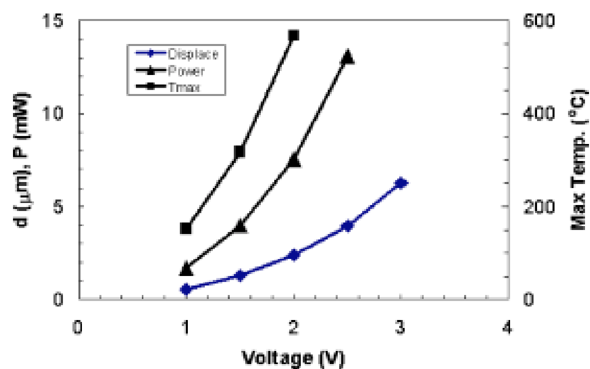

Fig. 4 Simulated displacement, power consumption, and T_{max} for a Si actuator as a function of bias. Very high temperature is required to produce a reasonable displacement, e.g., ~5 μm. The power needed is ~3 times higher than that of a Ni heatuator.

In order to investigate the average stress in the films, Ni was plated on a plain Cu seed layer that was sputter deposited on a Si substrate, whereas for gradient stress investigation and actuator fabrication, Ni films were plated by a through-mask plating technique.[21] A copper seed layer with a thickness of 50 nm was deposited on a SiO_2/Si substrate by sputtering, with a 5 nm Cr interlayer to increase the adhesion between the Cu and the substrate.

The photolithographic patterning process is as follows: positive photoresist AZ5214 was coated at a spin speed of 4000 rpm, which gave a typical thickness of ~1.4 μm. In order to obtain a thick resist mold for device fabrication, a second or a third layer of resist was used. After each coating, the sample was baked at 100 °C for 10 min; then the second or the third layer photoresist was coated at the same speed. Two layers of resist coating typically gave a mold thickness of 2–2.5 μm, depending on the baking time. The mold was baked at 110 °C for 2–5 min to increase the hardness and the adhesion of the mold to the substrate. Then the samples were mounted on a glass slide that contains an electrical path and conductive control area of 1 cm^2. As the device area is much smaller than the control area; the control area determines the current density. Optimized conditions of $J = 2-4$ mA/cm^2 and $T = 60$ °C were used to produce the actuator active material, with the residual stress minimized. After plating, the photoresist and the seed layer outside of the device area were removed by acetone and acid respectively, then the actuators were released by etching the Si substrate using a SF_6 reactive ion etching dry etch or a KOH solution (20 wt %) at 85 °C for ~30 min. The typical metal thickness for actuator devices is 1.5–2 μm.

Both the mean and the gradient residual stresses are important. For simplicity, the measured residual stress from a curved bilayer structure is called the average stress hereafter. The average residual stress is deduced from the curvature of a bilayer structure by applying Stoney's equation.[22] The curvatures of specimens before and after Ni plating were measured with a Dektak-8 instrument with a scan distance of 10 mm, and the difference was used to deduce the average residual stress.

For gradient stress investigation, cantilevers with various length (50–85 μm) and widths (15 and 25 μm) were used. After release by KOH etching, the cantilevers were typically bent due to the existence of the gradient stress. The deflection of the cantilevers was then measured using a ZYGO Corporation (Laurel Brook Road, Middlefield, CT 06455-0448, USA) optical interferometer. The gradient stress σ_g/t is related to the displacement y, of the cantilever tip by $\sigma_g/t = yE/L^2$.[23] Here L and t are the cantilever length and thickness. Young's modulus $E = 210$ GPa of bulk Ni was used for stress assessment, though the value of thin film Ni is slightly different and depends on the process conditions. From our beam bending experiments, the extracted E values from the Ni thin films plated at low current density are close to that of bulk one.[24]

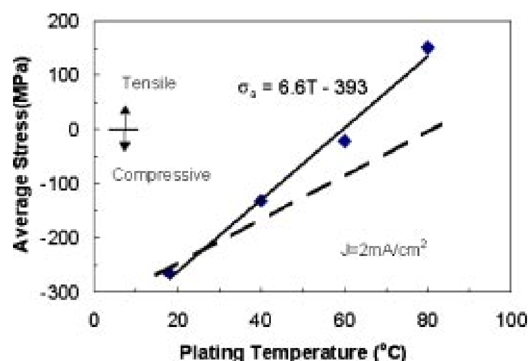

Fig. 5 The dependence of the average stress on plating temperature. The dashed line is the residual stress after extracting the thermal stress. It is dominated by compressive stress in the whole processing temperature region.

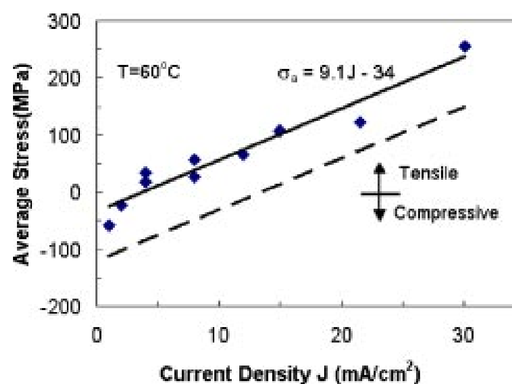

Fig. 6 The dependence of the average stress on the plating current density. The stress changes from compressive to tensile as the current density increases. The dashed line is the residual stress after extracting the thermal stress.

The resistance as a function of temperature was measured using thin wire structures with bond pads on both sides. These samples were plated on SiO_2/Si substrates without being released. Samples were mounted on a hot plate; and the temperature was controlled to 0.1 °C. Direct current was used to actuate the devices, and the displacements of the devices were measured by a video camera, and then analyzed. All actuator measurement was conducted at room temperature.

4 Results and Discussions

4.1 *Residual Stresses Control*

For MEMS applications, a stress-free thin film is essential. The residual stress of electroplated Ni films has been investigated as a function of temperature and current density. Figure 5 shows the dependence of the average stress on the plating temperature, in the range of 20–80 °C at a fixed current density of 2 mA/cm^2. The solid line is a linear fit to the measured data points. At $T \leqslant 60\,°C$, it is a compressive stress, the amplitude of the compressive stress decreases with increasing the temperature, and then changes to tensile at a temperature of 60 °C.

As the temperature increases, the plated Ni film expands more than the Si substrate as the thermal expansion coefficient of Ni film is $\alpha_{Ni} = 1.27 \times 10^{-5}/°C$ much larger than that of Si $\alpha_{Si} = 2.6 \times 10^{-6}/°C$. After plating and returning to room temperature, the Ni film contracts more than the Si substrate, leading to a concave bowing of the bilayer structure. The Ni film is then subjected to a tensile stress. The thermally generated tensile stress $\sigma_T = \Delta\alpha\Delta TE$, is linearly related to the temperature rise and the difference of thermal expansion coefficients, $\Delta\alpha$. The dashed line in Fig. 5 is the intrinsic residual stress after extracting the thermal stress, revealing that the remaining residual stress produced at low plating current density, is dominated by compressive stress, and the higher the plating temperature, the lower the average stress.

Figure 6 shows the dependence of the average stress on the plating current density from 1 to 30 mA/cm^2 at a fixed temperature $T = 60\,°C$. The average stress changes from mildly compressive to tensile; and the amplitude increases with increasing plating current density. The dashed line is the intrinsic residual stress after extracting the thermal stress, moving the zero stress regime toward higher current density. It can therefore be concluded that low current density produces a film with compressive stress, whereas high current density produces a film with tensile stress.

It is reasonable that slow plating produces a relatively denser film than fast plating, and atoms can migrate more at a higher temperature, and have sufficient time to move to relaxed positions. The film is dense with compressive stress. As the plating current density increases, the plating rate rises and the limited supply of Ni ions to the cathode leads to the formation of a depletion layer of Ni ions near the cathode surface: the so-called mass-transport limitation. The deposited layer is porous, rough, and possesses a tensile residual stress. It is known that the stress strongly depends on the plating conditions; a similar correlation to ours between stress and current has been reported elsewhere.[25,26]

Gradient stress behaves in different way from the mean stress. Ni cantilevers plated at a low temperature generally bend down much more than those plated at higher temperature. Figures 7(a) and 7(b) show the scanning electron microscopy (SEM) pictures of freestanding cantilevers released by KOH wet etching at 85 °C. The Ni thickness is 0.5–0.7 μm, and were plated at $J = 2$ mA/cm^2, at 20 and 60 °C, respectively. The cantilevers plated at 20 °C bend down severely due to the existence of the gradient stress, whereas those plated at 60 °C are straight with no visible curvature, indicating there is no gradient stress. Figure 8 shows the dependence of the gradient stress on the plating temperature at a fixed current density, $J = 4$ mA/cm^2. All the cantilevers bend downward, which means that the surface of the cantilevers is more compressive than the bottom of the cantilevers regardless of whether the average stress of the cantilevers is compressive or tensile stress. The amplitude of the gradient stress decreases with increasing plating temperature, and approaches zero at 60–80 °C for a plating current density of 4 mA/cm^2.

High temperature is responsible for the thermal tensile stress as shown previously, but high temperature plating leads to the relaxation of the film during plating. Ni atoms can migrate to relaxed positions, therefore the gradient stress tends to be zero at high temperature, consistent with the results of the above-mentioned average stress.

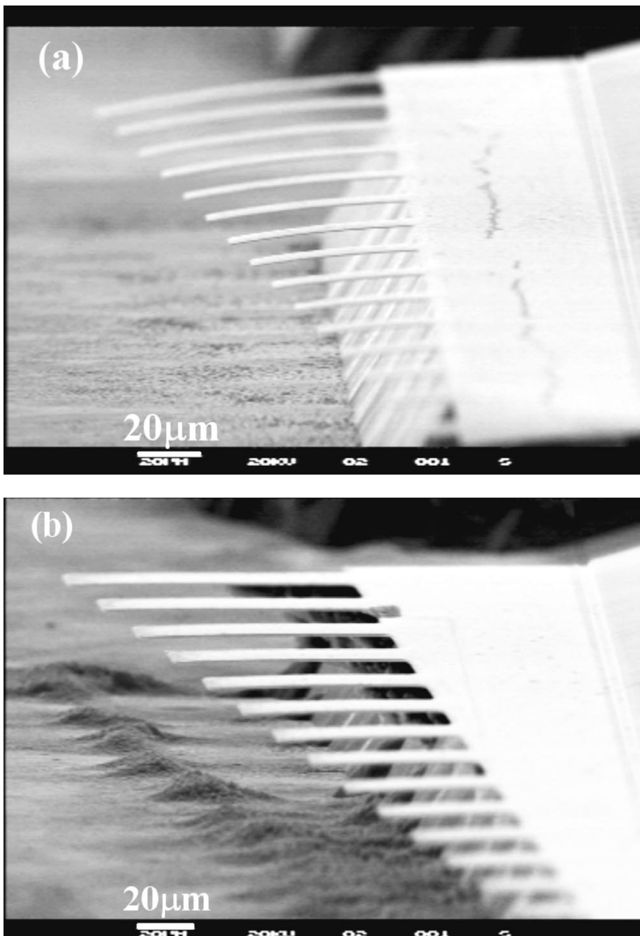

Fig. 7 SEM pictures of cantilever series released by KOH etching at 85 °C. Cantilevers plated at 20 °C. (a) Bend down due to existence of the gradient stress, whereas those plated at 60 °C. (b) Straight, with no curvature visible, indicating there is no gradient stress.

From the results of average and gradient stresses, it is understood that high temperature (60 °C) and low current density are the optimal conditions for stress-free Ni film deposition. These conditions were used for the actuator fabrication. The residual stress study suggests that plating $T = 80\,^\circ\mathrm{C}$ is better for zero gradient stress, however plating

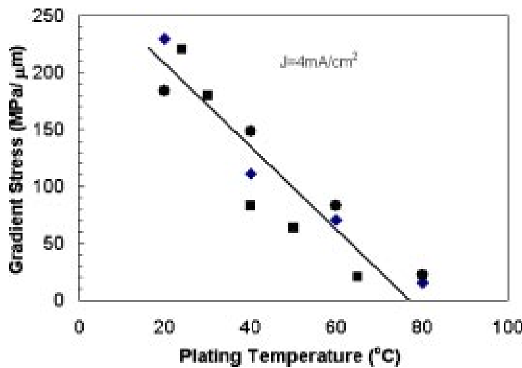

Fig. 8 The gradient stress as a function of temperature for three sets of experiments. The gradient stress diminished at a temperature round 60–80 °C.

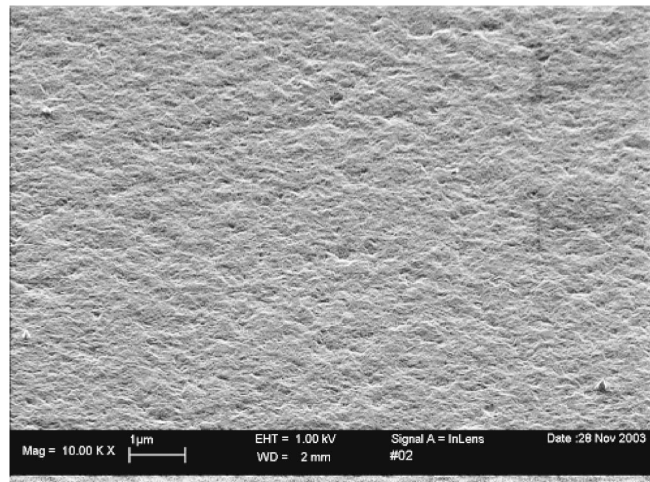

Fig. 9 SEM picture of electroplated Ni surface. The plating conditions are 40 °C and 4 mA/cm^2. The surface is very smooth with fine grain sizes.

at $T = 80\,^\circ\mathrm{C}$ corresponds to a hydrolysis process, which leads to the inclusion of the ammonium and sulfamate nonmetallic atoms in the films.[25] This makes the material elastic properties deteriorate significantly.[24,27] It has been confirmed that the plating speed at $T = 80\,^\circ\mathrm{C}$ is about 50% higher than those at $T \leqslant 60\,^\circ\mathrm{C}$ from our experiments, demonstrating that the hydrolysis reaction is occurring at $T = 80\,^\circ\mathrm{C}$, therefore $T = 60\,^\circ\mathrm{C}$ and $J = 2-4$ mA/cm^2 are the best conditions for the plating process to produce near zero stress Ni thin film materials.

4.2 *Resistivity and Young's Modulus*

The resistivity of electroplated Ni film has been measured for samples prepared at different plating current density and temperature. The resistivity values are in the range of 17–22 $\mu\Omega$ cm, about three times that of the bulk value 6.8 $\mu\Omega$ cm,[28] but do not vary significantly with plating current density and temperature.[27] A high resistivity for plated materials is not unexpected, as the plated material has more defects and impurities compared to bulk material. The independence of T and J of the resistivity means that the change of microstructures in plated materials is not sufficient to modify the electrical properties. We have inspected the surface of the Ni films by SEM and atomic force microscopy. The surface of Ni plated at room temperature or high current density is relatively rough with a root-mean square in the range of ~20 nm, down to ~11 nm as the temperature increased to 60 °C with current density <10 mA/cm^2. It seems that the resistivity is not affected by the observed grain size variation. Figure 9 is a typical SEM picture of electroplated Ni surface plated at 40–60 °C and 2–10 mA/cm^2. The surface is smooth with fine grain sizes. For the details of the plating uniformity and surface smoothness, please refer to Ref. 29.

Figure 10 shows the resistance $R(T)$ as a variation of temperature measured from a thin Ni wire on a SiO_2/Si substrate. The resistance increases linearly with the temperature. The normalized resistivity $[R(T) - R_0]/R_0 = [\rho(T) - \rho_0]/\rho_0$ against the temperature is shown in Fig.

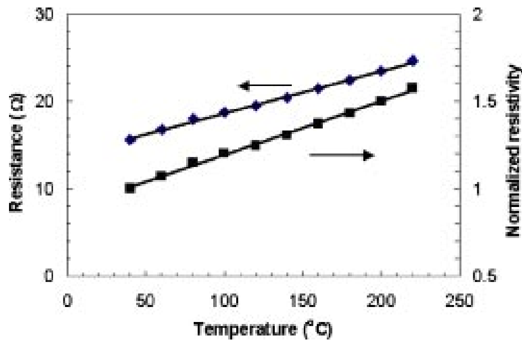

Fig. 10 The variation of resistance and its normalized resistivity as a function of temperature. The slope of the normalized resistivity gives the temperature coefficient of $3.0 \times 10^{-3}/°C$. The dimensions for the wire are $L/W/t = 580/7.5/1.04$ μm, respectively.

10, giving a temperature coefficient of the resistivity $\xi = 3.0 \pm 0.2 \times 10^{-3}/°C$. This coefficient is about twice that of the bulk value of $\xi = 1.5 \times 10^{-3}/°C$. The temperature coefficient for other samples plated at up to 30 mA/cm^2, have also been measured. They showed the same temperature coefficient of resistivity as shown previously, i.e., the temperature coefficient does not depend on the process conditions, consistent with the resistivity. The results imply that the electrical properties of electroplated Ni thin films do not correlate with the process conditions significantly.[27] The change in the resistivity and its temperature coefficient with plating conditions are expected for most of the plated materials as the plating produces materials with different microstructures from those of bulk ones.[30,31]

The Young's modulus of these plated Ni films has been investigated by a beam bending method.[24,32,33] The Young's modulus of these optimized Ni films is as high as 205 ± 40 GPa, close to that of bulk Ni material. However it decreases linearly from 205 to 85 GPa as the plating current densities were increased from 2 to 30 mA/cm^2.[24,27] The decrease of the Young's modulus is believed to be caused by changes in the material microstructure. Low current density plating correlates to a dense material; it becomes a less dense, sponge-like material, at high plating rates, corresponding to a low Young's modulus. The Young's modulus of those specimens plated at $T \leqslant 60\,°C$, is close to the bulk value, but drastically drops to $\sim$100 GPa as the plating temperature is raised to $80\,°C$.[24,27] The inclusion of nonmetallic ammonium and sulfamate is believed to be responsible for it.[25] In contrast to the electrical properties, the mechanical properties of electroplated Ni films strongly depend on the process conditions. The details of analysis and material properties of electroplated Ni thin films can be found from Refs. 24 and 27.

4.3 *Thermal Actuators and their MEMS Devices*

Lateral thermal actuators, switches, and microtweezers have been fabricated and tested electrically. The Ni layer for the actuators was plated at the optimal process conditions, i.e., 2–4 mA/cm^2 and $60\,°C$, unless otherwise specified. It was found that when the film thickness of active actuators is less than 0.8 μm, the hot arm of the heatuator tends to buckle up or down when voltage is applied instead of moving laterally. This is because a thin film could not produce sufficient force to deflect the heatuator laterally, but easily buckles vertically.[6] Therefore Ni film thickness of greater than 1.5 μm was used for all actuators. It is also reasonable to fabricate actuators with thick active material to generate sufficient force.

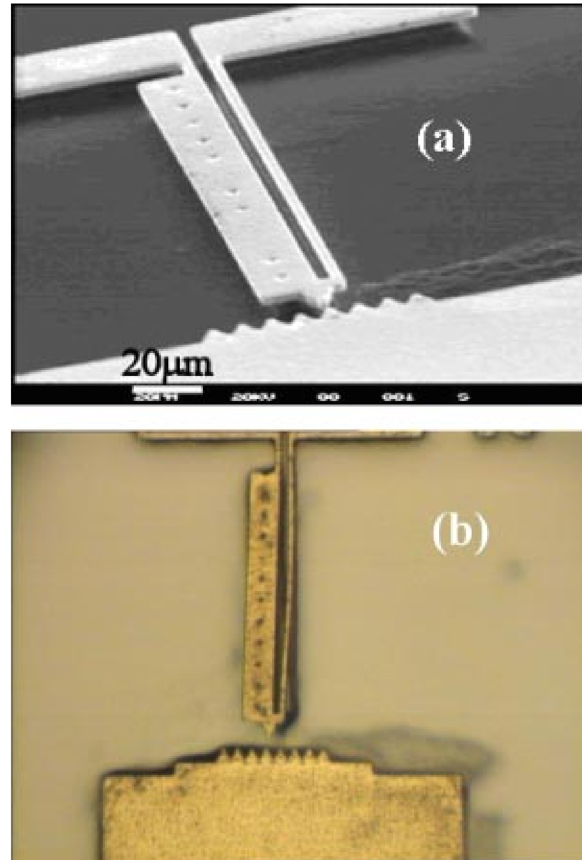

Fig. 11 A Ni heatuator (a) at zero bias (SEM picture) and (b) under a 36 mA dc, the heatuator deflected to the left side. The heatuator has arms lengths of $L_h/L_g = 160/20$ μm, and width of $W_h = 2$ μm. The distance between teeth is 8 μm.

Figure 11(a) shows a typical SEM picture of a freestanding Ni heatuator with $L_h = 180\,\mu$m. The device was released by SF_6 dry etch. The actuator is freestanding with no visible curvature, indicating the residual stress is near zero. Figure 11(b) shows the in-plane motion of the heatuator ($L_h/L_g = 160/20\,\mu$m) when a 36 mA current was applied. The heatuator clearly shows a large displacement, about $\sim$6 μm. The displacement and the electrical power have been investigated as a function of current density, as shown in Fig. 12. The displacement increases with increasing current density, in proportion to I^2, consistent with the analytic equation (5). At a current of 38 mA, the hot arm has been significantly heated up and deformed. Once deformed, the hot arm will not restore to its original position but remain at a backward position. This phenomenon has been also reported for poly-Si heatuators.[34] Further increasing the current leads to the burn-off of the hot arm, a permanent damage to the actuator. The power was calculated based on the current used and the voltage drop measured, which include the voltage drop on the bond pads. The resistance increases

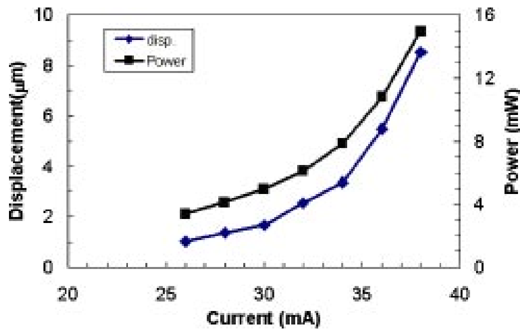

Fig. 12 Typical deflection and consumed power of a Ni heatuator as a function of dc. This heatuator has $L_h/L_g = 150/20\ \mu\text{m}$, respectively.

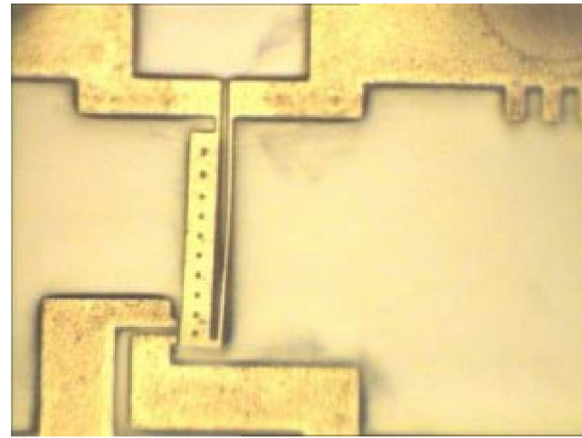

Fig. 14 A Ni microswitch with double contacts under 34 mA dc.

with increasing temperature as we expected for metal as discussed previously.

The response of a metal thermal actuator is fundamentally different from that of polysilicon when they are operated in a constant dc mode, due to the different signs in the temperature coefficients of resistivity, i.e., positive for metals and negative for polysilicon. For a resistor with a negative temperature coefficient, a dc decreases the resistance as the temperature increases, and less power is consumed. Whereas for a resistor with a positive temperature coefficient, a dc will increase the resistance of hot arm more than that of cold arm as the temperature rises, thus more power is consumed and heat dissipated. This could lead to thermal runaway of the hot arm, resulting in failure. Therefore, particular care has to be taken during the metal thermal actuator test. However most of the heatuator application is a relatively low temperature range so no runaway will occur. Figure 13 shows the deflections of the heatuators as a function of consumed power with device dimension as a parameter. The consumed power was calculated based on the current used and voltage measured. D1, D2, and D3 have the hot and cold arms lengths of $L_h/L_g = 160/10$, 160/20, and 150/30 μm, respectively, with other dimensions fixed as listed in Table 3. The displacement is proportional to the power used, consistent with the analytic equation (5). It is fundamentally important to know the operation temperature of the device. A rough estimation of the temperature can be obtained by measuring the average resistance change with the voltage as $R = R_0(1 + \xi\Delta T)$, ξ the temperature coefficient of the resistivity. From the $I-V$ characteristics, the average raised temperatures for these devices can be estimated to be within the range of 220–390 °C, corresponding to a maximum temperature of 330–590 °C of the devices, much lower than those of Si-based heatuators.

Figure 14 shows a micrograph of a microswitch utilizing the in-plane motion heatuator with double contacts. As the heatuator heats up, it makes contact with the two other electrodes, providing switch functionality. Metal heatuators can be effectively combined to make microtweezers, as they operate at a much lower temperature compared with Si-based devices. Figure 15 shows a SEM micrograph of a pair of microtweezers. The length and the width of the hot arm were 1100 and 10 μm, respectively. A dc of 35–50 mA was required to operate this pair of microtweezers. The displacement is not as big as anticipated owing to nonoptimized structure. Large microtweezers with millimetre dimensions using laser cutting and bulk Ni plate were reported, and a dc up to 1 A was required to operate the device,[35] which is too large for practical applications. Our small microtweezers, on the other hand, have shown the feasibility for small-scale applications.

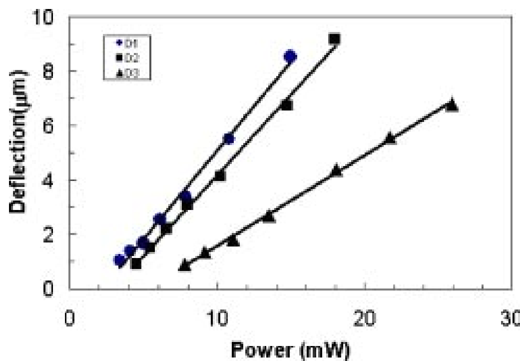

Fig. 13 Deflection as a function of consumed power for various heatuators. D1, D2, and D3 have the hot and cold arms lengths $L_h/L_g = 160/10$, 160/20, and 150/30 μm, respectively.

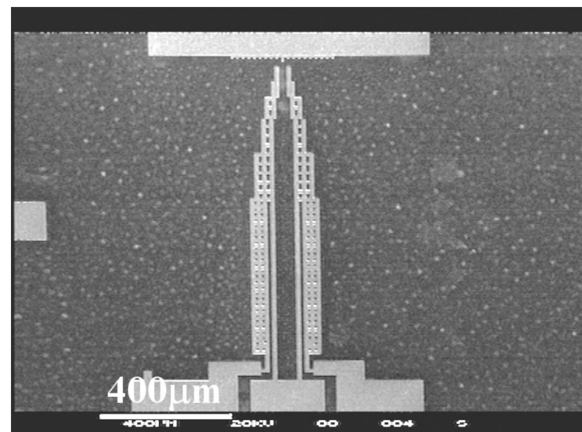

Fig. 15 A SEM micrograph of a pair of Ni microtweezers based on the in-plane motion thermal actuators. The length of the microtweezers and the width of the hot arm are 1100 and 10 μm, respectively.

5 Summaries and Conclusions

Metal-based actuators and sensors will play an important role in future MEMS applications, especially for those to be integrated with CMOS. Analysis has been performed to clarify the differences between metal- and Si-based actuators. Electroplated Ni was used to fabricate the thermal actuators. The key results can be summarized as follows.

- An analytical model has been established to analyze the heatuators based on Si and various metals. This showed that the deflections and the figure of merits, which solely depend on the material properties, for metals are much larger than those for a Si-based device.
- The positive temperature coefficient of electrical resistivity for metals makes the operation of thermal actuator more efficient than that of Si-based one, which typically has a negative temperature coefficient.
- Metal thermal actuators have much lower operating temperatures than polysilicon devices. They can generate a large displacement and force, suitable for integration with CMOS circuits. For a reasonable displacement, a polysilicon actuator typically needs to operate at a temperature higher than 900 °C, whereas metal actuators can operate in the range 200–400 °C.
- The residual differential stress of a plated Ni film can be controlled by adjusting the plating conditions. High temperature ($\sim$60 °C) and low current densities (2–4 mA/cm^2) resulting in relatively low plating rates are optimal conditions to obtain zero stress Ni film, suitable for MEMS fabrication.
- The resistivity of electroplated Ni is about three times that of bulk Ni, and its temperature coefficient is twice that of bulk Ni. These values are relatively insensitive to the process conditions.
- Lateral thermal actuators have been made by plating Ni and a mixture of surface and bulk processing techniques. Free standing, curvature free MEMS devices were obtained. Electrical testing has been performed. Lateral motion of heatuators has been observed. The displacement was found to increase linearly with increasing the power.

Acknowledgment

This project was sponsored by the Cambridge-MIT Institute under Grant No. 059/P.

References

1. W. D. Cowan and V. M. Bright, ''Vertical thermal actuator for micro-opto-electro-mechanical system,'' *Proc. SPIE* **3226**, 137–146 (1997).
2. J. R. Reid, V. M. Bright, and J. H. Comtois, ''Force measurements of polysilicon thermal micro-actuators,'' *Proc. SPIE* **2882**, 296–306 (1996).
3. T. Moulton and G. K. Ananthasuresh, ''Micromechanical devices with embedded electrothermal-compliant actuation,'' *Sens. Actuators, A* **90**, 38–48 (2001).
4. E. S. Kolesar, P. B. Allen, J. T. Howard, J. M. Wilken, and N. C. Boydston, ''Thermally actuated microbeam for large in-plane mechanical deflections,'' *J. Vac. Sci. Technol. A* **17**, 2257–2263 (1999).
5. Q. A. Huang and N. K. S. Lee, ''Analysis and design of polysilicon thermal flexure actuator,'' *J. Micromech. Microeng.* **9**, 64–70 (1999).
6. R. Hickey, M. Kujath, and T. Hubbard, ''Heat transfer analysis and optimization of two-beam microelectromechanical thermal actuators,'' *J. Vac. Sci. Technol. A* **20**, 971–974 (2002).
7. D. Koester, R. Mahedevan, and K. Marcus, ''Multi-user MEMS processes (MUMP) introduction and design rules,'' revision 3, *MCNC MEMS Technology Applications Centre*, Research Triangle Park, North Carolina (Oct. 1994).
8. S. D. Leith and D. T. Schwartz, ''High rate through-mold electrodeposition of thick (>200 um) NiFe MEMS components with uniform composition,'' *J. Microelectromech. Syst.* **8**, 384–392 (1999).
9. J. Gobet, F. Cardot, J. Bergqvist, and F. Rudolf, ''Electrodeposition of 3D microstructures on Silicon,'' *J. Micromech. Microeng.* **3**, 123–130 (1993).
10. W. H. The, J. K. Luo, M. A. Graham, A. Pavlov, and C. G. Smith, ''Near-zero curvature fabrication of miniaturized micromechanical Ni switches using electron beam cross-linked PMMA,'' *J. Micromech. Microeng.* **13**, 591–598 (2003).
11. S. Majumder, N. E. McGruer, and P. Zavracky, ''Electrostatically actuated micromechanical switches,'' *J. Vac. Sci. Technol. A* **15**, 1246–1249 (1997).
12. K. Kataoka, S. Kawamura, T. Itoh, K. Ishikawa, H. Honma, and T. Suga, ''Electroplating Ni micro-cantilevers for low contact-force IC probing,'' *Sens. Actuators, A* **103**, 116–121 (2003).
13. J. A. Wright and Y. C. Tai, ''Micro-miniature electromagnetic switches fabricated using MEMS technology,'' *Proc. 46th Annual Int. Relay Conf. NARM*, pp. 1231–1234, Oak Brook, Illinois (Apr. 1998).
14. S. Kawahito, Y. Sasaki, M. Ishida, and T. Nakamura, *Digest Tech. Papers, Transducers 93*, 888 (1993).
15. T. Hirano, T. Furuhata, and H. Fujita, *Digest Tech. Papers, Transducers 93*, 80 (1993).
16. C. S. Pan and W. Y. Hsu, ''An electro-thermal and laterally driven polysilicon microactuator,'' *J. Micromech. Microeng.* **7**, 7–13 (1997).
17. W. N. Sharpe, Jr., ''Mechanical properties of MEMS materials,'' Johns Hopkins University: Baltimore, Maryland (2001).
18. M. F. Ashby, *Materials Selection in Mechanical Design*, 2nd ed., Butterworth Heinemann, Boston (1999).
19. J. W. Gardner, *Microsensors: Principles and Applications*, Wiley, New York (1994).
20. H. P. Myers, *Introductory Solid State Physics*, Chapter 6, Taylor&Francis, London (1997).
21. R. V. Shenoy and M. Datta, ''Effect of mask wall angle on shape evolution during through-mask electrochemical micromachining,'' *J. Electrochem. Soc.* **143**, 544–549 (1996).
22. Marc J. Madou, *Fundamentals of Microfabrication*, Chapter 5, CRC Press, London/New York (2002).
23. S. D. Senturia, *Microsystem Design*, Chapter 9, Kluwer Academic, Boston/London (2001).
24. J. K. Luo, A. J. Flewitt, S. M. Spearing, N. A. Fleck, and W. I. Milne, ''The Young's modulus of electroplated Ni thin film for MEMS application,'' *Mat. Sci. Lett.* **58**, 2306–2309 (2004).
25. S. A. Watson, ''Compendium on nickel electroplating and electroforming,'' Ni Development Institute Tech. Series Reports 10047–10055 (1989).
26. J. C. Sadak and F. K. Sautter, ''Composition, mechanical properties and structure of electrodeposited cobalt-iron alloy,'' *J. Vac. Sci. Technol.* **11**, 771–776 (1974).
27. J. K. Luo, A. J. Flewitt, S. M. Spearing, N. A. Fleck, and W. I. Milne, ''Effects of plating process on the properties of electroplated Ni thin film'' (unpublished).
28. Alfa Aesar, *2003 Catalogue*, Research Chemicals Metals and Materials, p. 945, Johnson Matthey GmbH, Zeppelinstr, 7, D-76185 Karlsruhe, Germany.
29. J. K. Luo, D. P. Chu, A. J. Flewitt, S. M. Spearing, N. A. Fleck, and W. I. Milne, ''Uniformity control of Ni thin film microstructure deposited by through-mask plating,'' *J. Electrochem. Soc.* **152**, C36–41 (2005).
30. I. H. Ibrahim, A. K. Ibrahim, N. G. Gomaa, and S. F. Abaza, ''Surfactant effects on the electrical and thermal properties of $Ni_{76}P_{24}$ metallic glass alloy,'' *J. Phys.: Condens. Matter* **4**, 9501–9508 (1992).
31. S. C. Chang, J. M. Shieh, K. C. Lin, B. T. Dai, T. C. Wang, C. F. Chen, M. S. Feng, Y. H. Li, and C. P. Lu, ''Investigation of effects of bias polarization and chemical parameters on morphology and filling capability of 130 nm damascene,'' *J. Vac. Sci. Technol. B* **19**, 767–773 (2001).
32. P. Boyle, D. F. Moore, and R. R. A. Syms, ''Micropackaging using thin films as mechanical components,'' 52nd Electronic Component and Technology Conference (ECTC2002), San Diego.
33. Y. C. Tai and R. S. Muller, ''Measurement of Young's modulus on microfabricated structures using a surface profiler,'' *Digest, IEEE Micro Electro Mechanical Systems Workshop (MEMS90)*, Napa Valley, pp. 147–152 (1990).
34. D. Yan, A. Khajepour, and R. Mansour, ''Modelling of two-hot-arm horizontal thermal actuator,'' *J. Micromech. Microeng.* **13**, 312–322 (2003).
35. P. Lerch, C. K. Slimane, B. Romanowicz, and P. Renaud, ''Modelization and characterization of asymmetrical thermal micro-actuators,'' *J. Micromech. Microeng.* **6**, 134–137 (1996).

Jikui (**Jack**) **Luo** received his PhD degree from the University of Hokkaido, Engineering Faculty, Japan in 1989. From 1990 to 1995, he worked as a research associate and senior research fellow at Cardiff University, Wales, U.K. From 1995 to 2003 he worked as an engineer, senior engineer, and manager at Newport Wafer Ltd, Philips Semiconductor Co. and Cavendish Kinetics Ltd. He is presently a senior research member at the University of Cambridge, Engineering Department. His professional interests include advanced materials and devices for III–V semiconductors, CMOS, MOS power transistors, and microsystem. He currently conducts research in the development of microactuators using diamond-like carbon material and CMOS compatible MEMS.

Johnny H. He received his MSc in advanced material in micro-/nano-system from NUS and MIT of Singapore-MIT Alliance, and BEng in electrical engineering from Shanghai Jiao Tong University. He is currently working toward his PhD in MEMS at Cambridge University, Engineering Department. His research interest is in microfabrication, characterization, design and simulation of MEMS/NEMS. He is also a member of the Institute of Electrical Engineer (IEE), student member of the Institute of Electronics and Electrical Engineer (IEEE), and associate member of the Institute of Physics (IOP).

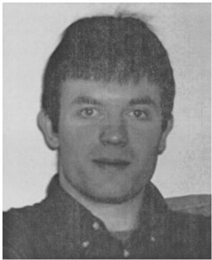

Andrew Flewitt earned his BSc in physics from the University of Birmingham in 1994. His PhD, completed in 1998, was undertaken in the Engineering Department, Cambridge University on the growth of hydrogenated amorphous silicon. He was appointed to a lectureship in the same institution in microelectromechanical systems in 2002, with particular research interests in novel materials and processing for MEMS applications.

D. F. Moore is a reader in Cambridge University, U.K., with research interests in microsystems (MEMS) technology; thin film materials and packaging applications; and electronic and superconducting devices. Prior to joining the faculty in Cambridge in 1984 he acquired his PhD in applied superconductivity at Stanford University, U.S.A., and worked five years in Bell Laboratories and in IBM Zurich.

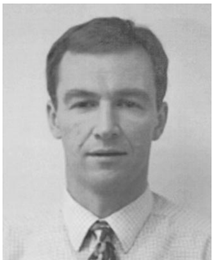

S. Mark Spearing received his PhD degree from Cambridge University, Engineering Department, in 1990. He is a professor of engineering materials at the University of Southampton, U.K., having been professor of aeronautics and astronautics at the Massachusetts Institute of Technology (MIT), Cambridge, U.S.A., where he served from 1994 to 2004. His technical interests include materials characterization, structural analysis and design of MEMS, development of new materials and processes for MEMS, packaging of microelectronic systems and MEMS, and the development of design approaches for advanced composites. Since 1995 he has been responsible for materials, structural design, and packaging tasks of the MIT MicroEngine, MicroRocket, Micro-Chemical Power, and MicroHydraulic Transducer projects as well as conducting crosscutting underpinning technology development.

Norman Fleck is a professor of mechanics of materials, and has been the Head of the Mechanics, Materials and Design Division of Cambridge University, Engineering Department since 1996. He is also the founder director of the Cambridge Center for Micromechanics, an interdisciplinary research center in engineering. He received his PhD in engineering (1984) in metal fatigue, and currently conducts research in the mechanics of engineering materials, including ferroelectrics, composites, foams, powder compaction, solid mechanics and engineering design. He has extensive experience in international research teams in the United States and in Europe, and runs a combined experimental/theoretical research group of about ten students and postdoctoral associates. He has about 190 journal publications, and consults for a number of small to medium sized companies, including a start-up company in drug delivery.

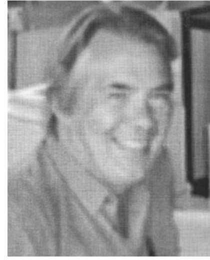

Bill Milne became head of the Electrical Engineering Division in Cambridge University in October 1999. He had previously obtained his BSc Hons (first class) in electrical engineering from St. Andrews University in 1970. He then went to Imperial College, London where he was awarded a DIC and PhD in electronic materials. In 1973 he joined the Plessey Company Research Laboratories at Caswell where he worked for three years on the anomolous diffusion effects in silicon and on high radiance infra-red LEDs. He joined the Engineering Department, Cambridge University as an assistant lecturer in 1976 and has since remained there. He was appointed to the Chair of Electrical Engineering in 1996 and is currently Head of the Semiconductor and Nanoscale Research Group consisting of 7 staff members, approximately 25 postdoctors, and 40 PhD students. His research interests include the production and application of amorphous and polycrystalline films and carbon nanotubes for use in both mechanical and electrical applications. He has published/presented over 475 papers/patents in these subjects.